Exacerbation of blood brain barrier dysfunction and brain injury after aneurysmal subarachnoid hemorrhage in endothelial specific S1PR1 knock out mice.

Akira Ito[1,4], Hui Yuan[1], Yunkyoung Lee[1], Gab Seok Kim[1, #], Giuseppe Faraco[2], Richard Proia[3], Kuniyasu Niizuma[4], Teiji Tominaga[4], Josef Anrather[2], Costantino Iadecola[2], Michael J Kluk[1] and Teresa Sanchez[1,2,*] .

[1]Department of Pathology and Laboratory Medicine, Center for Vascular Biology, Weill Cornell Medicine, New York, NY

[2]Department of Neuroscience, Brain and Mind Research Institute, Weill Cornell Medicine, New York, NY.

[3]Genetics of Development and Disease Branch, NIDK, NIH, Bethesda, MD.

[4] Tohoku University, Sendai, Japan

#Current address: Department of Neurology, UTHealth, McGovern Medical School, Houston TX.

* Correspondence to: Teresa Sanchez, PhD. Department of Pathology and Laboratory Medicine, Center for Vascular Biology, Department of Neuroscience, Brain and Mind Research Institute, Weill Cornell Medicine, 1300 York Ave, A607B, New York, NY 10065.

ABSTRACT

It is increasingly recognized that during ischemia, hypoxia and inflammation, blood brain barrier (BBB) dysfunction significantly contributes to the exacerbation of neuronal injury. Despite the therapeutic potential of the cerebrovascular endothelium, the limited understanding of the endothelial signaling pathways involved in blood brain barrier function restricts progress towards developing novel therapeutic approaches specifically targeting the endothelium in stroke. Sphingosine-1-phosphate (S1P) is a potent modulator of endothelial function via its receptors (S1PR). Recent human studies suggest that S1PR1 signaling is limiting in cardiovascular and inflammatory diseases. Herein, we aimed to investigate the expression of S1PR1 in the mouse and human brain and the role of endothelial-specific S1PR1 signaling in BBB function, neuronal injury and neurological outcomes in a mouse model of aneurysmal subarachnoid hemorrhage. We found that S1PR1 is the most abundant S1PR transcript in the mouse brain and in mouse and human brain endothelial cells (20-100 mRNA copies per cell). S1PR1 transcripts were significantly enriched (~6 fold) in mouse cortical microvessels compared to total brain. Using the S1PR1-eGFP knock in mouse, we found that S1PR1-eGFP is abundantly expressed in the cerebrovascular endothelium and neurons in the mouse cortex, hippocampus, corpus callosum and striatum. A similar pattern of expression was observed in human brain autopsy samples. Endothelial specific deletion of S1PR1, induced by tamoxifen administration in adult *S1pr1* $^{flox/flox}$*x Cdh5-Cre ERT2* mice, resulted in exacerbation of blood brain barrier dysfunction (albumin transcytosis), brain injury as well as worsened neurological outcomes upon subarachnoid hemorrhage compared to S1pr1 $^{flox/flox}$ littermates. No differences in bleeding upon rupture of the middle cerebral artery or in hemostasis, assessed in the tail bleeding assay were found.

Our studies indicate that lack of S1PR1 signaling in the endothelium exacerbates BBB dysfunction upon ischemic-hypoxic injury and thereby worsens neuronal injury and neurological outcomes. Given the expression of S1PR1 in the cerebrovascular endothelium in humans and recent findings indicating that S1P-S1PR1 anti-inflammatory signaling is limiting in cardiovascular disease and other inflammatory conditions, the therapeutic and diagnostic potential of this endothelial pathway in stroke is very high.

INTRODUCTION

Increasing preclinical and clinical data indicate the critical role of blood brain barrier (BBB) dysfunction in the pathophysiology of neurovascular ischemic, hypoxic and inflammatory injury, which occurs after stroke. For instance, the use and effectiveness of current therapies for ischemic stroke (i.e. tPA or mechanical rechanalization) are severely limited by the vascular complications of reperfusion injury (i.e. blood brain barrier dysfunction leading to vasogenic edema and hemorrhagic transformation)[1-5]. In hemorrhagic stroke, perihematoma edema volume expansion is associated with worsened outcomes [6]. In subarachnoid hemorrhage (SAH), blood brain barrier breakdown occurs in the acute phase and contributes to the exacerbation of neuronal injury [7-9]. However, currently, there are no therapies specifically targeting the endothelium to promote BBB function and prevent exacerbation of neurovascular injury in stroke. A better understanding of the cellular and molecular mechanisms governing BBB function may help design novel therapies aimed at restoring cerebral endothelial barrier function after stroke to prevent exacerbation of neurovascular injury and improve outcomes.

Sphingosine-1-phosphate (S1P) is a bioactive lipid, highly abundant in plasma and lymphatic fluids (within the range of several hundred nanomolar), which plays a critical role in vascular embryonic development [10]as well as endothelial and lymphocyte function[11] in adult mice *via* interaction with its receptors, S1PR. Although platelets store high amounts of S1P [12], the main sources of plasma S1P are erythrocytes [13] and endothelial cells [14, 15]. In plasma, S1P is bound to albumin and HDL *via* its ligand Apolipoprotein M, which protects S1P from degradation[16, 17]. S1P receptors (S1PR) bind their ligand within the low nanomolar range (the K_D of S1P for S1PR ranges from 8-27nM) [18-20]. Since S1P levels are very high in plasma and very low in tissue, and endothelial cells are one the main sources of plasma S1P, S1PR signaling is

predominant in the endothelium compared to other tissues[21]. In endothelial cells, the most abundant S1PR transcript is S1PR1. We and others have shown that S1P via S1PR1 promotes endothelial integrity and inhibits endothelial activation in a G_i-phosphatidylinositol-3-kinase (PI3K)-Akt-eNOS dependent way[22, 23 24, 25]. This anti-inflammatory pathway contributes to the cardiovascular protective effects of HDL [26, 27]. Recent studies indicate that S1P anti-inflammatory and vasoprotective signaling via S1PR1 could be limiting in human cardiovascular and inflammatory diseases [28-31 25]. For instance, in coronary artery disease, the content of ApoM or S1P in the HDL fraction is significantly reduced, and it inversely correlates with the severity of the disease[28, 29]. In addition, in diabetic patients, ApoM levels are significantly decreased compared to non-diabetic [32, 33]. Given these findings, in this study we aim to investigate the expression of S1PR1 in the mouse and human brain and the role of endothelial S1PR1 signaling in blood brain barrier dysfunction and brain injury upon subarachnoid hemorrhage. Our results underscore the critical role of S1PR1 endothelial signaling in blood brain barrier function and stroke outcomes and highlight the therapeutic potential of the endothelium in stroke.

METHODS

Mice. All animal experiments were approved by the Weill Cornell Institutional Animal Care and Use Committee. Endothelial cells specific *S1pr1* knockout mice (*S1pr1*$^{flox/flox}$ *Cdh5–Cre*^{ERT2}*;* referred to as *S1pr1*^{iECKO}) were generated as described [34]. *S1pr1*$^{flox/flox}$ mice [35] were crossed to *VE-Cadherin-Cre*^{ERT2} mice (provided by Ralph Adams) [36] to generate *S1pr1*$^{flox/flox}$ *VE-Cadherin-Cre*^{ERT2} mice. Mice were treated with tamoxifen (Sigma-Aldrich, cat. no. T5648) by oral gavage (75 mg kg^{-1}) for 3 days at the age of 8 weeks and used for the experiments 3-4 weeks after tamoxifen treatment. *S1pr1*$^{flox/flox}$ littermates treated with tamoxifen were used as control mice. All experiments were performed in male mice.

Endovascular perforation SAH surgery. SAH surgery was performed on C57/BL6/J, *S1pr1*^{iECKO} mice and their littermate *S1pr1*^{iECKO} controls as we have previously described [37]. In brief, surgery was performed using a dissecting surgical microscope. Temperature was maintained at 36.5–37.5 °C by using a thermostatic blanket (Harvard Apparatus, CMA 450 Animal Temerature Controller) throughout the procedure. Mice were anesthetized with isoflurane inhalation delivered by facemask in 100% of O_2. A 15 mm midline vertical incision was made on the skin in the head. The head was fixed in stereotactic frame and cerebral blood flow was measured by Laser-speckle imager (PeriCam PSI system, Perimed, Sweden). During surgery, mice were in supine position. A 10 mm midline vertical incision was made on the skin in the neck. The common carotid, external carotid and internal arteries were dissected from the adjacent tissue. The superior thyroid artery and the occipital artery were cauterized and cut. The external carotid artery was sutured with a dead knot and cauterized above the suture. A second suture loop was also placed in the external carotid artery just before the bifurcation of the common carotid artery. A slit-knot was placed around the common carotid artery. A small clip was applied to the internal carotid artery and the slip-knot around the common

carotid artery was tightened temporally. A small incision was made in the external carotid artery stump. A 5-0 monofilament (Covidien, cat. no. 1741-21) was inserted into the incision and the knot around the external carotid artery was tightened to prevent bleeding. Then, the monofilament was advanced to the common carotid artery, the small clip on the internal carotid artery was removed and the monofilament was guided through the external carotid artery to the internal carotid artery. The knot around the common carotid artery was opened again and the monofilament was introduced to the bifurcation of the internal carotid artery. The monofilament was gently push less than 1 mm further and quickly withdrawn to the external carotid artery. The knot around the external carotid artery was loosen and the monofilament was slowly removed. The external carotid artery was quickly ligated to prevent bleeding. The mouse was turned in prone position and induction of subarachnoid hemorrhage was confirmed by reduction of cerebral blood flow by Laser-speckle contrast imager. After the surgery, all animals were maintained in a small animal heated recovery chamber. Two different severities of SAH models were created by changing the tip shapes of 5-0 monofilament; a round tip for severe SAH mode, a flat tip for mild SAH model. The surgeon and the investigator conducting the analysis were blinded to the genotype of the mice. Animals which did not exhibit a reduction in CBF upon endovascular rupture were excluded from the study.

RNA isolation, reverse transcription and quantitative PCR analysis (RT-qPCR)

Total RNA from mouse brains and cells was prepared using RNeasy Mini Kit (Qiagen, Valencia, CA) as instructed by the manufacturer. To generate cDNA, 100 ng of RNA was reverse transcribed using random primers and SuperScript II RT-polymerase (Invitrogen, Carlsbad, CA). Primers were designed using the Primer Express oligo design program software (Applied Biosystems, Foster City, CA). Real-time quantitative PCR was performed using the SYBR Green I assay on the ABI 7500 Sequence Detection System (Applied Biosystems). PCR reactions for each cDNA sample were performed in

duplicate and copy numbers were calculated using standard curves generated from a master template as we previously described. The sequence of the primers used for qPCR are shown in Table 2.

S1PR1 Immunohistochemistry

Human tissues were retrieved from Brigham and Women's Department of Pathology archives; this work was approved by the Institutional Review Board (Protocol #2013P001431).

Immunohistochemistry for S1PR1 was performed on an automated stainer (Leica Bond III, Leica Biosystems, Buffalo Grove, IL) using an anti-human S1PR1 rabbit polyclonal antibody (Santa Cruz Biotechnology Inc.) at a final concentration of 1.3 ug/ml. The IHC technique for S1PR1 was validated as we have previously described [38]. 5μm formalin fixed paraffin embedded tissue sections of human frontal cortex were deparaffinized and processed using heat induced epitope retrieval with an EDTA-based buffer (Leica #AR9640) for 20 minutes and incubated with primary antibody for 30 minutes at room temperature. Secondary antibody (polymer) incubation (10 minutes) and diaminobenzidine-based signal generation (10 minutes) were performed per manufacturer's instructions (Leica # DS9800). Pictures were taken using SPOT Insight Gigabit camera and SPOT Imaging Software (5.1).

Immunofluorescence staining

C57BL/6 male mice and S1pr1-eGFP knock in [50] (26-30 g) were used for the study. Under deep anesthesia, mice were perfused with cold PBS and subsequently with 4% PFA in PBS solution. The brains were removed, postfixed with 4% PFA for 24 h, transferred to 30% sucrose solution in PBS, embedded in OCT media and frozen. Coronal sections were cut (30 μm) in a cryostat and immunofluorescence was conducted in floating sections. Sections were preserved at -20^{0}C in a PBS solution containing 30% polyethylene glycol and 30% sucrose. Sections were washed three

times with Tris-buffered saline (TBS) and were then blocked with TBS-blocking solution (1 % bovine serum albumin, 0.2 % skim milk, and 0.3 % Triton X-100 in TBS) for 1 h and incubated with the specified primary antibodies in TBS-blocking solution overnight on a shaker at 4 °C, followed by the appropriate secondary antibodies for 2 hours at room temperature. Brain slices were stained with 4',6-diamidino-2-phenylindole (DAPI) for 7 minutes and were mounted onto slides. Samples were observed on a Zeiss LSM 510 Meta Confocal microscope (Carl Zeiss Microscopy, Thornwood, NY). Images were captured using Zen LE software (Carl Zeiss Microscopy).

Isolation of cortical microvessels. The brain microvessels were isolated as we have previously described [34, 39]. All procedures were performed in a cold room. The brains were collected and rinsed in MCDB131 medium (Thermo Fisher Scientific, cat. no. 10372019) with 0.5% fatty acid-free BSA (Millipore Sigma, cat. no.126609). The leptomeninges, cerebellum, brainstem and white matter were removed on ice. The cortices were homogenized in 8 mL of MCDB131 medium with 0.5% fatty acid-free BSA using a 7-mL loose-fit Dounce tissue grinder (Sigma-Aldrich, cat. no. D9063) with 10 strokes. The homogenates were centrifuged at 2,000 g for 5 min at 4 °C. The pellet was suspended in 15% dextran (molecular weight ~70,000 Da, Sigma-Aldrich, cat. no. 31390) in PBS and centrifuged at 10,000 g for 15 min at 4 °C. The pellet was resuspended in MCDB131 with 0.5% fatty acid-free BSA and centrifuged at 5,000 g for 10 min at 4 °C. The pellet contained the brain microvessels.

Protein extraction from brain microvessels and western blotting. Brain microvascular fragments were lysed in HEPES-RIPA buffer (50 mM HEPES pH 7.5; 1% Triton; 0.5% sodium deoxycholate; 0.1% SDS; 500 mM NaCl; 10 mM MgCl2; 50 mM β-glycerophosphate) with 1x Protease inhibitor cocktail (CalBiochem, cat. no. 539131), 1 mM Na3VO4 and 1 mM NaF and centrifuged at 15,000 r min^{-1} for 15 min. Equal amount of proteins were mixed with SDS sample buffer, boiled and separated on a 4-15%

polyacrylamide gel (Bio-Rad, cat. no. 4561084), transferred to PVDF membranes (Millipore Sigma, cat. no. IPVH00010), and blocked 5 % milk in 0.1% Tween-20 in TBS. Immunoblot analysis was performed with S1PR1 (1:250; Santa Cruz, cat. no. sc25489) and β-actin (1:1,000; Santa Cruz, cat. no. sc-1616 HRP) antibodies. Membrane were washed with 0.1% Tween-20 in TBS, incubated with anti-rabbit IgG secondary antibody conjugated to horseradish peroxidase (1:2,000; Cell Signaling, cat. no. 7074S), and protein bands were visualized with enhanced chemilumescent (ECL) reagent (Thermo Fisher Scientific, cat. no. 32106) on a Protec OPTIMAX X-Ray Film Processor. Relative band intensities were obtained by densitometric analysis of images using ImageJ software.

Brain endothelial cells isolation and assessment of deletion efficacy of endothelial *S1pr1*. After two weeks after tamoxifen treatment, a mouse was sacrificed and the brain was collected and rinsed in MCDB131 medium (Thermo Fisher Scientific, cat. no. 10372019) with 0.5% fatty acid-free BSA (Millipore Sigma, cat. no.126609). The cortices were homogenized in MCDB131 medium using a 7-mL loose-fit Dounce tissue grinder (Sigma-Aldrich, cat. no. D9063) with 15 strokes. The homogenate was mixed with same amount of 30% dextran (molecular weight ~70,000 Da, Sigma-Aldrich, cat. no. 31390) in PBS and centrifuged at 4,500 r min^{-1} for 15 min at 4 °C. The pellet was resuspended in MCD131 medium and centrifuged at 2,400 r min^{-1} for 10 min. The pellet was resuspended in Liberase TM solution (3.5 U; Roche, cat. no. 5401119001) with DNaseI (0.4 U; AppliChem Inc, cat. no. A3778) and digested at 37.0 °C for 90 min. The enzymatic reaction was stopped by adding 2 mM of EDTA and 2% of BSA. After centrifugation at 2,400 r min^{-1} for 10 min, the pellet was incubated in purified Rat Anti-Mouse CD31antibody (MEC13.3) (1 : 100; BD Biosciences, cat. no. 550274) with Dynabeads Sheep Anti-Rat IgG (Invitrogen, cat. no. 11035) for 35 min. CD31 positive endothelial cells were isolated by using DynaMag-2 Magnet (Thermo Fisher Scientific,

cat. no.12321D). Total RNA was extracted from the isolated endothelial cells using shredder (Qiagen, cat. no. 79654) and RNeasy Mini Kit (Qiagen, cat. no. 74106) with RNase-free DNase treatment (Qiagen, cat.no. 79254) according to the manufacturer's instructions. Reverse transcription was carried out using Verso cDNA Synthesis Kit (Thermo Fisher Scientific, cat.no. AB1453B). Real-time PCR was performed on a real-time PCR system (Applied Biosystems, ABI 7500 Fast) by using PerfeCTa SYBR Green Fast Mix Low ROX (cat.no. AB1453B). PCR primer sequences for target molecules are in Table 2.

Grading system for SAH. Blood volume in the subarachnoid space was assessed using the grading system previously reported [40]. Mice were sacrificed under deep anesthesia 24 h after SAH induction and the brains were removed. Pictures of ventral surface of the brain depicting the basal cistern with the circle of Willis and the basilar artery were taken using a stereomicroscope (Olympus, SZX16) equipped with digital camera (Olympus, DP12). The basal cistern was divided into 6 segments and a grade from 0 to 3 was given to each segment: Grade 0, no subarachnoid blood; Grade 1, minimal subarachnoid blood; Grade 2, moderate blood clot with recognizable arteries; Grade 3, blood blot obliterating all arteries. Blood volume was evaluated by a total score ranging from 0 to 18 from six segments.

Tail bleeding assay. Tail bleeding time was determined as described previously[41]. A mouse was anesthetized with a mixture of ketamine and xylazine, and body weight was measured. The mouse was placed on a heating pad in prone position, the tail tip was about 4 cm blow the body horizon. A distal 5 mm segment of the tail was amputated, and the tail was immediately immersed in PBS pre-warmed at 37 °C. The time to complete arrest of bleeding was determined: complete arrest is no blood flow for 1 minute. The blood volume was determined by hemoglobin assay. Blood cells were separated by centrifuge at 4,000 r/min for 5 min at room temperature, and erythrocytes

were resuspended in BD Pharm Lyse (BD Biosciences, cat. no. 555899). After 10 min incubation in the buffer, the lysate was centrifuged at 10,000 r/min for 5 min. Hemoglobin concentrations were measured spectrophotometrically at 550 nm using a plate reader (Molecular Devices, SpectraMax M2e).

Mortality and neurological outcome. Mortality was assessed at 24, 48 and 72 hours after SAH induction. Gross neurological outcome was blindly evaluated before and at 24, 48 and 72 hours after surgery by sensorimotor scoring as described previously [42, 43]. Briefly, a motor score (0 to 12; spontaneous activity, limb symmetry, climbing, and balance) and a sensory score were used [42, 43]. Gross neurological outcome was evaluated by a total score of 4 to 24. Higher scores indicate better neurological outcome.

Brain water content. Brain edema was determined by using the wet/dry method as previously described [44]. Mice were sacrificed at 72 hours after surgery and the brains were quickly removed and separated into the left and right cerebral hemispheres and weighed (wet weight). The brain specimens were dried in an oven at 55°C for 72 hours and weighed again (dry weight). The percentage of water content was calculated as ([wet weight-dry weight]/wet weight) x 100%.

Cell death detection. DNA strand breakage during apoptosis after SAH was assessed by phospho-histon H2A.X (Ser 139) immunofluorescence as previously described [45]. Because phosphorylation of histon H2A.X at Ser 139 (γ-H2AX) is abundant, fast, and correlates well with each DNA strand breakage, it is the most sensitive marker that can be used to examine the DNA damage [46]. Mice were deeply anesthetized and perfused with cold PBS and subsequently with 4% PFA in PBS solution. The brains were removed, post-fixed with 4% PFA for 24 h and transferred to 30% sucrose solution. Frozen brains were cut with a 10 μm of thickness by a cryostat (Leica, CM3050 S). The brain slices were blocked with TBS- blocking solution (5% bovine serum albumin and 0.5% Tween 20 in PBS) for 1 hour at room temperature and incubated with phospho-

histone H2A.X (Ser 139) (20E3) antibody (1:100; Cell Signaling, cat. no. # 9718S) in blocking solution overnight on a shaker at 4 °C. Sections were washed three times with 0.5% Tween 20 in PBS and then incubated with goat anti- rabbit IgG Alexa- 488 (1:200; Life Technologies, cat. no. A-11008). DAPI (40 ,6-diamidino-2-phenylindole) staining was used as a counter staining. Sections were imaged by using an FluoView FV10i confocal microscope (Olympus, Japan) (original magnification, x 40). For quantification, the percentage of phospho-histon H2A.X positive cells per DAPI positive cells from three different fields in the ipsilateral cerebral cortex area per mouse (bregma -1.64 to -1.28 mm) were counted and the average values were plotted.

Assessment of blood brain barrier dysfunction. Small macromolecules (≤ 3 kDa) leakage from the blood into the brain parenchyma was assessed using dextran–tetramethylrhodamine (TMR) (3-kDa) dye (Thermo Fisher Scientific, cat. no. D3308) Dextran-TMR (3-kDa) extravasation experiments were performed as described with modifications [34, 47, 48]. Mice were anesthetized and Dextran-TMR (3-kDa) (10 μg g^{-1}) was injected in the external jugular vein 22 hours after surgery. After 2 hours circulation, mice were deeply anesthetized and perfused with cold PBS to remove intravascular dye. The ipsilateral hemispheres were removed and homogenized in 1% Triton X-100 in PBS. The lysate was centrifuged at 15,000 r min^{-1} twice for 15 min at 4 °C, and the supernatant was used to measure fluorescence (excitation/ emission = 540/590 nm, SpectraMax M2e, Molecular Devices). The relative fluorescence values (R.F.U.) were normalized by the brain weights.

To assess albumin extravasation, evans blue dye (EBD) was used because EBD binds to plasma albumin[49]. Mice were anesthetized and 2% EBD (4 ml kg^{-1}) was injected in the external jugular vein 21 hours after surgery. After 3 hours circulation, mice were deeply anesthetized and perfused with cold PBS to remove intravascular dye. The ipsilateral hemispheres were removed and homogenized in 50% trichloroacetic acid in PBS. The

lysate was centrifuged at 15,000 rpm min^{-1} twice for 15 min at 4 °C, and the supernatant was used to measure fluorescence (excitation/ emission = 620/680 nm, SpectraMax M2e, Molecular Devices). The relative fluorescence units (R.F.U.) were normalized by the brain weights.

Transient middle cerebral artery occlusion (tMCAO)

All animal studies were approved by the Beth Israel Deaconess Medical Center and the Weill Cornell Medicine Institutional Animal Care and Use Committees and were in accordance with the guidelines established by the NIH.

Transient focal cerebral ischemia was induced by using the intraluminal suture model in mouse (tMCAO) as we have previously described [52]. Mice were anesthetized with 3 % isoflurane and then the anesthesia was maintained at 2% isoflurane during the surgeries. The rectal temperature was controlled at 37°C with a homeothermic pad. Before the surgeries, the surgical area was disinfected with povidone-iodine. A midline neck incision was made, and the left common carotid artery (CCA), left internal common carotid artery (ICA) and external common carotid artery (ECA) were exposed. The hole was made on the ECA, and the 6-0 surgical monofilament nylon suture with a round tip (approximately 0.22 mm diameter) was introduced into the left ICA through the hole of the ECA to block the blood flow to the MCA. Blood flow in the MCA territory was monitored throughout the procedure using a laser Doppler probe (PeriFlux system 5000, Ardmore, PA, USA), placed on the skull directly over the territory of the left MCA perfusion area. Reperfusion was established by the removal of suture after 60 minutes of MCA occlusion. For sham controls, the same procedures were done except that the suture was not inserted. After the surgery, all animals were maintained in a small animal heated recovery chamber (IMS Vetcare Chamber Recovery Unit, Harvard Apparatus, Holliston, MA).

2, 3, 5-triphenyltetrazolium chloride (TTC) staining and determination of infarct volume

Twenty hours after transient ischemia, brains were carefully removed and were put on brain matrices to slice into 1-mm coronal sections. The slices were then incubated in 2 % TTC solution (Sigma Aldrich, MO) for 30 minutes at room temperature, followed by the fixation with 4% paraformaldehyde (PFA). The slices were scanned and infarct area on each slice was determined by using Image analysis software (Image J, the National Institutes of Health, Bethesda, MD) to obtain the infarct ratios, edema ratios and infarct volumes per brain (in mm^3). Infarct areas were calculated by using the following equation to correct for edema formation in the ischemic hemisphere: I=X-Y, where X is the area of the contralateral (nonischemic)

hemisphere and Y is the area of the intact regions of the ipsilateral (ischemic)

hemisphere. Infarct ratios were obtained after normalization by the contralateral hemisphere. Edema ratios were calculated with the following formula: E=(Z−X)/X, where Z is the area of the ipsilateral hemisphere. Direct infarct volume was obtained by integrating measured damaged areas as previously described [53]. Infarction volume was expressed as mm^3.

Statistical analysis. All results were expressed as mean ± SEM. Statistical analysis were performed with GraphPad Prism (GraphPad Software, Version 7.0c) by using two-tailed Student's t-test, one-way analysis of variance (ANOVA) followed by Tukey's test or two-way ANOVA followed by Bonferoni's test. *P* values < 0.05 were considered statistically significant.

RESULTS

Abundant expression of S1PR1 in the mouse and human brain

We first investigated the expression of S1PR in total brain homogenates, mouse primary neurons and mouse brain endothelial cells by reverse transcription and quantitative PCR analysis (RT-qPCR), as we have previously described [38, 54]. We found that S1PR1 was robustly expressed in the mouse brain *in vivo*, (Fig. 1A, 20.5± 2.4 copies/10^6 18S, which is equivalent to approximately 20.5± 2.4 S1PR1 mRNA copies/cell [55]), as well as in the mouse brain endothelial cell line bEnd.3 [56] (Fig. 1B, 87.3±2.9 copies/cell), primary mouse neurons (Fig. 1C, 16.4±1.3 copies/cell) and mouse primary mixed glial cells (Fig. 1D, 8.3±0.15 copies/cell) *in vitro.* Then, we used an optimized method to isolate cerebral microvessel fragments from mouse cortex [39] and compared the expression of S1PR1 in brain microvessels to the expression in total brain. Interestingly, we found that S1PR1 transcripts are highly enriched in brain microvessels when compared to total brain (Fig. 1E, ~6 fold enrichment in microvessels *vs* whole brain).

Using the S1pr1-eGFP knock in mice, in which endogenous S1PR1 has been replaced by the S1PR1-eGFP fusion protein [50], we found that S1PR1 is abundantly expressed in the cerebrovascular endothelium all throughout the brain (Fig. 2A, B) as assessed by detection of S1PR1-eGFP and immunofluorescence (IF) analysis for Glut-1. S1PR1 is also expressed in cortical (Fig. 2C) and hippocampal (Fig. 2D) neurons *in vivo*, both in the neuronal somas and the neuropil, as assessed by co-staining with MAP-2 (Fig. 2C and D) and Nissl (not shown). In addition, in some GFAP positive cells weak S1PR1-eGFP signal was detected, suggesting that lower levels of S1PR1 were expressed in astrocytes compared to neurons or brain endothelial cells (not shown). Similar pattern of expression was observed in the mouse brain when immunofluorescence analysis was

conducted using a S1PR1 specific antibody previously validated in our laboratory [38] (data not shown)

In order to investigate the expression of S1PR1 in the human brain, we conducted IHC analysis in sections from the frontal lobe of a total of 5 brain autopsy samples (Figure 3). The S1PR1 antibody and IHC protocol used in human samples were previously validated in our laboratory [38]. We observed a very similar pattern of S1PR1 expression in these 5 samples. S1PR1 immuno positivity was observed both in the grey matter (GM) and white matter (WM) areas (Figure 3A, low magnification). S1PR1 was widely detected in the cerebrovascular endothelium in the grey matter, white matter and pial vessels (Fig. 3A-F). More specifically, we detected S1PR1 in the endothelium of pial vessels (cerebral arteries and veins) (Fig. 3C), as well as in arterioles (Fig. 3D), capillaries (Fig. 3E and F) and venules (Fig. 3E) in the brain parenchyma. In the grey matter, S1PR1 staining was observed in neuronal bodies and in the neuropil (Fig. 3B, C).

Altogether, our data indicate that from all S1PR, S1PR1 is the most abundant S1PR transcript in brain, brain endothelial cells and neurons. S1PR1 protein is also widely detected in the mouse and human brain, mainly the cerebrovascular endothelium and neurons. S1PR1 transcripts are highly enriched in mouse cerebral microvessels versus total brain.

Lack of S1pr1 in the endothelium results in worsened outcomes in the acute phase of SAH

In order to investigate the role of endothelial S1PR1 signaling in the pathophysiology of aneurysmal SAH, we first used the endovascular rupture model of SAH in wild type mice [37]. 24 hours after SAH, we isolated microvessels from the mouse cortex and to determine sphingosine 1-phosphate receptor 1 (S1PR1) protein level compared to sham mice. We found that S1PR1 protein levels were detected by western blot assay in

cerebral microvessels in sham animals. We also detected a modest increase in S1PR1 levels, at 24 hours and 48 hours after SAH (1.68 ± 0.19-fold and 1.26 ± 0.05-fold, respectively) which was statistically significant (Fig.4A). Given these data and the abundant expression of S1PR1 in the cerebrovascular endothelium in the mouse and human brain, we aimed to investigate the role of endothelial specific S1PR1 in early brain injury (EBI) after SAH. We generated endothelial specific S1PR1 mice (S1PR1 iECKO) by treating adult *S1pr1*$^{flox/flox}$ *Cdh5–Cre*^{ERT2} mice (~2 month old) with 75 mg kg^{-1} of tamoxifen for 3 consecutive days (Fig.4B). *S1pr1*$^{flox/flox}$ littermate mice were also treated and used as wild type control (S1PR1 WT). We assessed the efficiency of deletion in S1PR1 iECKO by isolating brain endothelial cells from mice 2 weeks after tamoxifen treatment. RT-qPCR analysis demonstrated ~90% reduction of *S1pr1* expression in *S1pr1*^{iECKO} mice compared to *S1pr1*$^{flox/flox}$ littermate mice treated with tamoxifen in the same manner (Fig. 4B).

S1pr1^{iECKO} and *S1pr1*$^{flox/flox}$ littermate mice were subjected to SAH surgery using a rounded suture to induce severe SAH [37]. Mortality at 24, 48 and 72 hours after SAH was significantly higher in *S1pr1*^{iECKO} mice (40, 60 and 60%, respectively) compared to *S1pr1*$^{flox/flox}$ (10, 10 and 10%, at 24, 48 and 72 hours, respectively) (Fig. 4C).

Then, *S1pr1*^{iECKO} and *S1pr1*$^{flox/flox}$ mice were subjected to a milder SAH model by changing the shape of tip of nylon suture to perforate the cerebral artery. *S1pr1*^{iECKO} mice exhibit a trend towards a higher mortality rate (26.3, 26.3 and 26.3% in *S1pr1*^{iECKO} versus 7.7, 7.7 and 7.7% in *S1pr1*$^{flox/flox}$, at 24, 48 and 72 hours after SAH, respectively)(Fig. 4D), although it was not statistically significant. In addition, we found that *S1pr1*^{iECKO} mice exhibited statistically significant worsen neurological outcomes at 24h and 48h after SAH (16.29 ± 1.37, 17.14 ± 1.40, respectively) compared to *S1pr1*$^{flox/flox}$ mice (20.91 ± 0.81 and 21.00 ± 0.83) (Fig. 4E). Given the high mortality rate in

S1pr1^{iECKO} subjected to the severe SAH model, we used the milder SAH for subsequent studies.

These data indicate that endothelial specific deletion of S1PR1 exacerbates brain injury in the acute phase of SAH and increases mortality rate.

Genetic deletion of *S1pr1* in the endothelium has no effect on hemostasis or bleeding after SAH.

Since the amount of subarachnoid blood correlates with outcome after SAH [57] [40]we assessed the amount of subarachnoid blood upon SAH (by a SAH grading system, previously described [40]) and hemostasis (by tail bleeding assay [41]) and in *S1pr1*^{iECKO} and *S1pr1*$^{flox/flox}$ mice. No significant differences were observed in the amount of subarachnoid blood between *S1pr1*$^{flox/flox}$ and *S1pr1*^{iECKO} mice at 24h (Fig. 5A). SAH grading, determined by image analysis as previously described [40] was 11.50 ± 0.62 in *S1pr1*$^{flox/flox}$ mice and 11.67 ± 0.42 in *S1pr1*^{iECKO}. Consistent with the subarachnoid blood volume data, we did not find any significant differences in the bleeding times or blood volumes in the tail bleeding assay between *S1pr1*$^{flox/flox}$ and in *S1pr1*^{iECKO} mice. Bleeding times were 68.88 seconds ± 4.98 in *S1pr1*$^{flox/flox}$ and 63.8 seconds ± 4.14 in *S1pr1*^{iECKO} (Fig. 5C) and blood volumes, assessed by hemoglobin content were 0.73 ± 0.07 in *S1pr1*^{iECKO} mice compared to 0.70 ± 0.12 in *S1pr1*$^{flox/flox}$ mice (Fig. 5D). These data indicate that hemostasis is not impaired in *S1pr1*^{iECKO} with regards to wild type and the amount of blood in the subarachnoidal space upon SAH is similar in wild type and *S1pr1*^{iECKO} *mice.*

We also determined cerebral blood flow (CBF) changes during SAH in both groups of mice by Laser-Speckle flowmetry. Cerebral blood flow in the middle cerebral artery (MCA) territory rapidly dropped 1 minute after SAH in the ipsilateral side (to 31.65 ± 3.46% of basal in *S1pr1*^{iECKO} and to 40.26 ± 4.09% of basal in *S1pr1*$^{flox/flox}$) and the

contralateral side (to 82.42 ± 3.72% of basal in *S1pr1*^{iECKO} and to 77.32 ± 3.90% of basal in *S1pr1*$^{flox/flox}$), and recovered to ~85% of basal 2 h after SAH in the ipsilateral side (to 87.46 ± 7.15% in *S1pr1*^{iECKO} versus to 82.83 ± 5.88% in *S1pr1*$^{flox/flox}$) and ~95 to 100% in the contralateral side (102.81 ± 1.97% in *S1pr1*^{iECKO} versus 95.34 ± 4.86% in *S1pr1*$^{flox/flox}$) both *S1pr1*^{iECKO} and *S1pr1*$^{flox/flox}$ mice (Fig. 5E). These data indicate that genetic deletion of *S1pr1* in the endothelium did not significantly impact CBF changes during SAH.

Finally, no significant differences were observed in the physiological parameters (arterial O_2 saturation, heart rate, pulse distention and respiratory rate) between *S1pr1*^{iECKO} and *S1pr1*$^{flox/flox}$ mice, before or after SAH (Table 1).

Altogether, these data indicate that lack of S1PR1 in the endothelium increases mortality and worsen neurological outcomes in the acute phase after SAH, without having an impact on bleeding, cerebral blood flow changes or systemic physiological parameters such as heart rate, respiratory rate, O_2 saturation or pulse distension, which is a surrogate of pulse pressure.

Endothelial specific deletion of *S1pr1* in adult mice exacerbates blood brain dysfunction after SAH.

In animal models of ischemic and hypoxic neurovascular injury, BBB disruption is an early event in the pathophysiology of neurovascular ischemic injury. Two distinct cellular mechanisms of BBB dysfunction have been shown to be important in stroke. Studies using endothelial specific genetic manipulations have shown that the endothelial cytoskeleton *via* stress fibers formation plays a critical role in the early breakdown of the BBB by allowing the passage of small molecules (i.e. 3kDa dextran) through the junctions[48] (i.e. paracellular pathway). In addition, increased endothelial transcytosis [58]

(e.g. albumin transport via the transcellular pathway) [47] also contributes to BBB dysfunction.

In order to discern between these 2 possible mechanisms of BBB dysfunction upon SAH, we used two different tracers, 3-kDa dextran–tetramethylrhodamine (TMR) dye as small size tracer which crosses the BBB via the paracellular pathway [47, 48] and Evans blue dye, which binds to plasma albumin, and therefore enters the brain parenchyma via endothelial transcytosis [58]. 24 hours after SAH, we observed significant leakage of both 3KDa TMR-dextran and albumin into the brain parenchyma in wild type mice (Fig 6A and B, 3.41 ± 0.47 and 1.53 ± 0.06 fold SAH versus wild type sham, respectively). Albumin transcytosis after SAH was significantly higher in *S1pr1*^{iECKO} mice with regards to wild type (1.83 ± 0.08 in *S1pr1*^{iECKO}, 1.53 ± 0.06 in *S1pr1*$^{flox/flox}$*, Fig. 6B).* Consistent with our recently published studies [34], 3KDa TMR-dextran leakage was increased in sham *S1pr1*^{iECKO} with regards to wild type (3.55 ± 0.80 in *S1pr1*^{iECKO} , 1.00 ± 0.11 in wild type litter mates, Fig. 6A). Interestingly, small molecule BBB leakage was not further increased upon SAH in *S1pr1*^{iECKO} *(*3.00 ± 0.20 fold induction after SAH in *S1pr1*^{iECKO}, Fig. 6A*)*.

These data indicate that after SAH, BBB dysfunction occurs both via the paracellular and the transcellular pathway. In addition, albumin transcytosis after SAH was significantly increased in mice lacking S1PR1 in the endothelium.

Endothelial deletion of *S1pr1* exacerbates brain edema and cell death after SAH. In order to determine the impact of the lack of endothelial S1PR1 on brain injury after SAH, we assessed brain edema at 72 hours after mild SAH surgery by quantifying total brain water content. *S1pr1*$^{flox/flox}$ mice (82.83 ± 0.53%) had slightly higher brain water content in ipsilateral hemisphere compared to sham (81.34 ± 0.20%) (Fig. 7A). Interestingly, brain edema was significantly increased in *S1pr1*^{iECKO} mice (84.39 ±

0.91%) compared to the wild type (Fig. 7A). There was no increase in brain water content in contralateral hemisphere in neither of three groups.

Next, we analyzed cell death at 24 hours after SAH using phospho-histone H2A.X (Ser 139) immunostaining, a marker for DNA fragmentation resulted from apoptosis. We found that *S1pr1*^{iECKO} mice showed significantly higher numbers of phospho-histone H2A.X positive cells compared to *S1pr1*$^{flox/flox}$ mice (50.85 ± 2.56% in *S1pr1*^{iECKO} versus 34.00 ± 2.98% in *S1pr1*$^{flox/flox}$) (Fig. 7B and C).

These data indicate that endothelial specific deletion of *S1pr1* worsens total brain edema and cell death, thereby contributing to poorer outcomes after SAH.

Endothelial specific *S1pr1 null mice* exhibit bigger infarcts, exacerbated total cerebral edema and worsened neurological outcomes after ischemic stroke.

In order to investigate the role of endothelial S1PR1 signaling in ischemic stroke, we induced transient cerebral focal ischemia in wild type and *S1pr1*^{iECKO} using the tMCAO model, as we have previously described [52, 59]. Similar to the SAH model, we did not observed significant changes in the physiological parameters and cerebral blood flow before, during ischemia or after reperfusion, between wild type and *S1pr1*^{iECKO}. Endothelial specific genetic deletion of S1PR1 in adult mice (S1pr1 iECKO mice) significantly exacerbated neuronal injury 24 h after tMCAO (infarct sizes were 46.9±3.8 mm3 in wild type and 75.4±7.7 mm3 in S1pr1 iECKO mice, ~63% bigger, Fig. 8A). Also, total cerebral edema was significantly higher (~46%) after ischemic stroke (total edema ratios were 0.098± 0.007 in wild type and 0.143±0.01 in S1pr1 iECKO mice, Fig. 8B). Neurological deficits at 24 h were significantly worse in S1pr1 iECKO mice compared to wild type littermates (Fig. 8C). These data indicate that lack of S1PR1 in the endothelium exacerbates brain injury and cerebral edema upon ischemic stroke.

ACKNOWLEDGEMENTS

This work was supported by internal funds provided by the Departments of Surgery and Emergency Medicine, BIDMC, the Department of Pathology and Laboratory Medicine, Weill Cornell Medicine, American Heart Association Grant-in-Aid 12GRNT12050110, NIH HL094465 and Leducq Foundation grants to TS.

We would like to thank Dan Li and Dr. Shou-ching Jaminet from the Multi-Gene Transcriptional Profiling Core Facility (Center for Vascular Biology Research, Beth Israel Deaconess Medical Center, Harvard Medical School) for the quantitative PCR analysis and Dr. Louise McCullough (University of Connecticut School of Medicine) for her input in the project.

The authors declare no competing financial interests.

FIGURE LEGENDS

Figure 1. S1PR1 mRNA is the most abundant S1PR transcript in brain, brain endothelial cells and neurons and it is highly enriched in brain microvessels. S1PR mRNA levels in A) normal mouse brain, B) the mouse brain endothelial cell line bEnd.3, C) primary mouse neurons and D) primary mouse mixed glial cells. E) Comparison of S1PR1 mRNA levels in whole brain versus brain microvessels. Quantitative reverse transcription and polymerase chain reaction (qRT-PCR) demonstrates that S1PR1 transcript is predominant over the other S1PR and it is highly expressed in brain microvessels. B) Log scale. The individual values and the mean ± SEM are shown. N=3-6. *$p<0.05$.

Figure 2. S1PR1 expression in the mouse brain in S1PR1-eGFP knock in mice. S1PR1-eGFP fluorescence confocal analysis in the mouse brain. A), B) S1PR1-eGFP is expressed in the cerebrovascular endothelium (green channel). Immunofluorescence for Glut-1 (endothelial marker) is shown in the red channel. Two examples of microvessels in the corpus callosum are shown. Scale bar 10μm. C), D) S1PR1-eGFP in cortex and hippocampus. S1PR1-eGFP is expressed in neurons and the neuropil (green channel). Immunofluorescence for MAP-2 (neuronal marker) is shown in the red channel. Scale bar 20μm. Representative pictures are shown. N=5-6.

Figure 3. S1PR1 expression in the human brain. Representative images of S1PR1 immunohistochemistry in 5 human brain autopsy samples. Formalin-fixed paraffin-embedded tissue sections were used for immmunohistochemical staining of S1PR1, as described in the Methods section. A) Expression of S1PR1 in the white and grey matter. Scale bar 500 μM. B) Representative picture showing S1PR1 immunopositivity in the neuropil, arterioles and capillaries of the grey matter. C) Detection of S1PR1 in the cerebrovascular endothelium of pial vessels. D-F) Representative pictures of the white

matter. Notice S1PR1 positivity in parenchymal arteries (D) and arterioles (F), venules (E) and capillaries (E,F). B-F) Scale bar 50 μM.

Figure 4. Increased mortality and worsened outcomes after SAH in endothelial specific S1pr1 null mice. A) Western blot analysis for S1PR1 in brain microvessels after SAH. 24 and 48 hours after subarachnoid hemorrhage (SAH) cortical microvessels were isolated and S1PR1 levels were detected by western blot (n = 4). Representative immunoblot image and quantification of S1PR1. βactin bands are used as a loading control and for normalization in quantification. $^{**}P < 0.01$, One-way ANOVA followed by Tukey's test. B) *S1pr1*$^{flox/flox}$ and *S1pr1*^{iECKO} mice were treated with tamoxifen (75 mg kg^{-1}) for the consecutive 3 days at the age of 8 weeks. *S1pr1* mRNA expression levels were analyzed by qPCR in brain endothelial cells isolated from *S1pr1*$^{flox/flox}$ and *S1pr1*^{iECKO} mice 2 weeks after tamoxifen treatment (n = 4). Deletion efficacy of endothelial specific *S1pr1* in *S1pr1*^{iECKO} is shown relative to *S1pr1*$^{flox/flox}$ mice. $^{**}P < 0.01$, Student's t-test. C) Survival curves after severe SAH surgery in *S1pr1*$^{flox/flox}$ and *S1pr1*^{iECKO} mice (n = 10). D) Survival curves after mild SAH surgery *S1pr1*$^{flox/flox}$ and *S1pr1*^{iECKO} mice (n = 13 or 19). C and D) Log-rank test. E) Neurological deficits after mild SAH surgery in *S1pr1*$^{flox/flox}$ and *S1pr1*^{iECKO} mice (n = 12 or 14). From 4 to 24 points: 24 points (best), 4 points (worst). Data are mean ± s.e.m. $^{*}P < 0.05$, $^{**}P < 0.01$, One-way ANOVA followed by Tukey's test. Red line, *S1pr1*^{iECKO}; Blue line, *S1pr1*$^{flox/flox}$.

Figure 5. Subarachnoid blood volume, hemostasis and CBF changes after SAH in *S1pr1*$^{flox/flox}$ and *S1pr1*^{iECKO} mice. A) Representative images of the ventral side of the brain depicting the basal cistern from *S1pr1*$^{flox/flox}$ and *S1pr1*^{iECKO} mice at 24 hours after SAH. B) SAH grade was calculated by quantifying the blood in the subarachnoidal space by image analysis as described in methods section. C) Quantification of blood amount in the subarachnoid space (n = 6). C) and D) Tail bleeding assay for hemostasis: C)

bleeding time and D) blood volume (n = 8). (B-D) Student's t-test. B-D individual values and mean±SEM are shown. (E) Superficial CBF in the middle cerebral artery territory was measured by Laser-speckle contrast imager in in *S1pr1*$^{flox/flox}$ and *S1pr1*^{iECKO} mice before (0 min.), 1 min, 10 min, 2 h, 4 h, 24 h after SAH induction. The relative CBF values (%) versus before SAH are shown. Data are mean ± SEM. (n = 6). Two-way ANOVA followed by Bonferoni's test showed no statistically significant differences between wild type and *S1PR1*^{iECKO}. Red solid line, *S1PR1*$^{flox/flox}$ ipsilateral side; blue solid, *S1PR1*^{iECKO} ipsilateral; light dotted line, *S1PR1*$^{flox/flox}$ contralateral; light blue dotted line, *S1PR1*^{iECKO} contralateral. IL, ipsilateral side. CL, contralateral side.

Figure 6. Endothelial specific S1pr1 null mice exhibit exacerbated BBB leakage (albumin transcytosis) after SAH compared to wild type litter-mates. A) 3-kDa dextran-TMR leakage 24 hours after sham or SAH surgery in *S1pr1*$^{flox/flox}$ and *S1pr1*^{iECKO} mice (n = 5 - 8). Dextran-TMR dye was circulating for 2 hours. B) Evans blue dye leakage (albumin transcytosis) 24 hours after sham or SAH surgery in *S1pr1*$^{flox/flox}$ and *S1pr1*^{iECKO} mice (n = 6 - 10). Evans blue dye was circulating for 3 hours. The individual values and mean ± SEM are shown. *P < 0.05, **P < 0.01, ***P < 0.001 (One-way ANOVA followed by Tukey's test). y axis shows relative fluorescence units (R.F.U.) per gram of tissue.

Figure 7. Exacerbated cerebral edema and neuronal injury after SAH in endothelial specific S1pr1 null mice A) 72 hours after SAH, brain edema was evaluated by brain water content in *S1pr1*$^{flox/flox}$ and *S1pr1*^{iECKO} mice (n = 7 - 14). Brain water content was calculated as ([wet weight-dry weight]/wet weight) x 100. * p<0.05, one-way ANOVA followed by Tukey's test. B) Immunofluorescence confocal analysis of phospho-histone H2A.X (DNA damage, green channel). Nuclear staining (DAPI) is shown in the blue channel. Representative images of ipsilateral hemisphere (cortex) from *S1pr1*$^{flox/flox}$ and *S1pr1*^{iECKO} mice after SAH stained are shown. Scale bar, 50 μm. C) Quantification of

phospho-histone H2A.X positive cells (%) (n = 7 or 8 mice). *$P < 0.05$, student's t-test. The individual values and the mean ± SEM are shown.

Figure 8. Exacerbated brain injury, cerebral edema and worsened neurological outcomes in *S1pr1*^{iECKO} compared to *S1pr1*$^{flox/flox}$ after ischemic stroke.

Focal transient ischemia was induced in ***S1pr1***$^{flox/flox}$ and ***S1pr1***^{iECKO} mice by MCAO (60 minutes) as described in the method section. 24 after reperfusion neurological deficits were determined and TTC staining was conducted to quantify infarct size and edema ratio by image analysis. A) Infarct volumes, B) Edema ratio and C) Neurological scores (4=worst, 0=best) were determined as described in method section. The individual values and the mean±SEM are shown. *P<0.05, **$P < 0.01$, Mann-Whitney U test.

Table 1. Physiological variables in *S1pr1*$^{flox/flox}$ and *S1pr1*^{iECKO} mice.

Time points	Parameters	*S1pr1*$^{flox/flox}$	*S1pr1*^{iECKO}
5 min before SAH	Arterial O_2 saturation (SpO_2, %)	98.6 ± 0.2	98.4 ± 0.1
	Heart rate (b.p.m.)	442.0 ± 23.2	459.2 ± 10.7
	Pulse distention (μm)	13.8 ± 0.7	12.8 ± 0.9
	Respiratory rate (br.p.m.)	162.3 ± 4.9	155.0 ± 6.7
5 min after SAH	Arterial O_2 saturation (SpO_2, %)	98.6 ± 0.1	98.6 ± 0.2
	Heart rate (b.p.m.)	539.8 ± 9.9	549.7 ± 9.9
	Pulse distention (μm)	13.2 ± 1.1	12.5 ± 0.9
	Respiratory rate (br.p.m.)	133.3 ± 4.4	126.8 ± 6.5

bpm, beats per minute; br.p.m., breaths per minute. Pulse distention is a surrogate for pulse pressure (pulse pressure 1⁄4 systolic pressure diastolic pressure). No significant differences were observed in the physiological parameters (arterial O_2 saturation, heart rate, pulse distention and respiratory rate) between *S1pr1*$^{flox/flox}$ and *S1pr1*^{iECKO} mice, before and after SAH

Table 2. Sequences of the primers used for RT-qPCR	
Target Genes	**Primer's Sequences**
Mouse S1PR1	F: CCGGATCGTATCTTGTTGCA R: AAATTCCATGCCTGGGATGA
Mouse S1PR2	F: ATGGGCGGCTTATACTCAGAG R: GCGCAGCACAAGATGATGAT
Mouse S1PR3	F: GCCTAGCGGGAGAGAAACCT R: CCGACTGCGGGAAGAGTGT
Mouse S1PR4	F: TTAGAGTGGTCCGAGCCAATG R: GATCATCAGCACGGTGTTGAGT
Mouse S1PR5	F: CACCGGCAGTCCTGGAGTA R: AAGGGTTGGGAAGCGTCAGT
18S	F: ACCTCTCGAAGTGTTGGATACAG R: TTCACTAATGACACAAACGTGATTC

REFERENCES

1. Saver JL. Improving reperfusion therapy for acute ischaemic stroke. *J Thromb Haemost*. 2011;9 Suppl 1:333-343
2. Molina CA, Alvarez-Sabin J. Recanalization and reperfusion therapies for acute ischemic stroke. *Cerebrovasc Dis*. 2009;27 Suppl 1:162-167
3. Hamann GF, Okada Y, del Zoppo GJ. Hemorrhagic transformation and microvascular integrity during focal cerebral ischemia/reperfusion. *J Cereb Blood Flow Metab*. 1996;16:1373-1378
4. Ames A, 3rd, Wright RL, Kowada M, Thurston JM, Majno G. Cerebral ischemia. Ii. The no-reflow phenomenon. *Am J Pathol*. 1968;52:437-453
5. del Zoppo GJ, Mabuchi T. Cerebral microvessel responses to focal ischemia. *J Cereb Blood Flow Metab*. 2003;23:879-894
6. Murthy SB, Moradiya Y, Dawson J, Lees KR, Hanley DF, Ziai WC, Butcher K, Davis S, Gregson B, Lyden P, Mayer S, Muir K, Steiner T. Perihematomal edema and functional outcomes in intracerebral hemorrhage. *Influence of Hematoma Volume and Location*. 2015;46:3088-3092
7. Macdonald RL, Pluta RM, Zhang JH. Cerebral vasospasm after subarachnoid hemorrhage: The emerging revolution. *Nature clinical practice. Neurology*. 2007;3:256-263
8. Macdonald RL. Delayed neurological deterioration after subarachnoid haemorrhage. *Nat Rev Neurol*. 2014;10:44-58
9. Pluta RM, Hansen-Schwartz J, Dreier J, Vajkoczy P, Macdonald RL, Nishizawa S, Kasuya H, Wellman G, Keller E, Zauner A, Dorsch N, Clark J, Ono S, Kiris T, Leroux P, Zhang JH. Cerebral vasospasm following subarachnoid hemorrhage: Time for a new world of thought. *Neurol Res*. 2009;31:151-158
10. Liu Y, Wada R, Yamashita T, Mi Y, Deng CX, Hobson JP, Rosenfeldt HM, Nava VE, Chae SS, Lee MJ, Liu CH, Hla T, Spiegel S, Proia RL. Edg-1, the g protein-coupled receptor for sphingosine-1-phosphate, is essential for vascular maturation. *J Clin Invest*. 2000;106:951-961
11. Matloubian M, Lo CG, Cinamon G, Lesneski MJ, Xu Y, Brinkmann V, Allende ML, Proia RL, Cyster JG. Lymphocyte egress from thymus and peripheral lymphoid organs is dependent on s1p receptor 1. *Nature*. 2004;427:355-360
12. Yatomi Y, Ruan F, Hakomori S, Igarashi Y. Sphingosine-1-phosphate: A platelet-activating sphingolipid released from agonist-stimulated human platelets. *Blood*. 1995;86:193-202
13. Pappu R, Schwab SR, Cornelissen I, Pereira JP, Regard JB, Xu Y, Camerer E, Zheng YW, Huang Y, Cyster JG, Coughlin SR. Promotion of lymphocyte egress into blood and lymph by distinct sources of sphingosine-1-phosphate. *Science*. 2007;316:295-298
14. Venkataraman K, Lee YM, Michaud J, Thangada S, Ai Y, Bonkovsky HL, Parikh NS, Habrukowich C, Hla T. Vascular endothelium as a contributor of plasma sphingosine 1-phosphate. *Circ Res*. 2008;102:669-676
15. Fukuhara S, Simmons S, Kawamura S, Inoue A, Orba Y, Tokudome T, Sunden Y, Arai Y, Moriwaki K, Ishida J, Uemura A, Kiyonari H, Abe T, Fukamizu A, Hirashima M, Sawa H, Aoki J, Ishii M, Mochizuki N. The sphingosine-1-phosphate transporter spns2 expressed on endothelial cells regulates lymphocyte trafficking in mice. *J Clin Invest*. 2012;122:1416-1426
16. Murata N, Sato K, Kon J, Tomura H, Yanagita M, Kuwabara A, Ui M, Okajima F. Interaction of sphingosine 1-phosphate with plasma components, including

lipoproteins, regulates the lipid receptor-mediated actions. *Biochem J*. 2000;352 Pt 3:809-815
17. Christoffersen C, Obinata H, Kumaraswamy SB, Galvani S, Ahnstrom J, Sevvana M, Egerer-Sieber C, Muller YA, Hla T, Nielsen LB, Dahlback B. Endothelium-protective sphingosine-1-phosphate provided by hdl-associated apolipoprotein m. *Proc Natl Acad Sci U S A*. 2011;108:9613-9618
18. Lee MJ, Van Brocklyn JR, Thangada S, Liu CH, Hand AR, Menzeleev R, Spiegel S, Hla T. Sphingosine-1-phosphate as a ligand for the g protein-coupled receptor edg-1. *Science*. 1998;279:1552-1555
19. Sato K, Ui M, Okajima F. Differential roles of edg-1 and edg-5, sphingosine 1-phosphate receptors, in the signaling pathways in c6 glioma cells. *Brain Res Mol Brain Res*. 2000;85:151-160
20. Kon J, Sato K, Watanabe T, Tomura H, Kuwabara A, Kimura T, Tamama K, Ishizuka T, Murata N, Kanda T, Kobayashi I, Ohta H, Ui M, Okajima F. Comparison of intrinsic activities of the putative sphingosine 1-phosphate receptor subtypes to regulate several signaling pathways in their cdna-transfected chinese hamster ovary cells. *J Biol Chem*. 1999;274:23940-23947
21. Kono M, Tucker AE, Tran J, Bergner JB, Turner EM, Proia RL. Sphingosine-1-phosphate receptor 1 reporter mice reveal receptor activation sites in vivo. *J Clin Invest*. 2014;124:2076-2086
22. Lee MJ, Thangada S, Claffey KP, Ancellin N, Liu CH, Kluk M, Volpi M, Sha'afi RI, Hla T. Vascular endothelial cell adherens junction assembly and morphogenesis induced by sphingosine-1-phosphate. *Cell*. 1999;99:301-312
23. Morales-Ruiz M, Lee MJ, Zollner S, Gratton JP, Scotland R, Shiojima I, Walsh K, Hla T, Sessa WC. Sphingosine 1-phosphate activates akt, nitric oxide production, and chemotaxis through a gi protein/phosphoinositide 3-kinase pathway in endothelial cells. *J Biol Chem*. 2001;276:19672-19677
24. Sanchez T, Estrada-Hernandez T, Paik JH, Wu MT, Venkataraman K, Brinkmann V, Claffey K, Hla T. Phosphorylation and action of the immunomodulator fty720 inhibits vascular endothelial cell growth factor-induced vascular permeability. *J Biol Chem*. 2003;278:47281-47290
25. Sanchez T. Sphingosine-1-phosphate signaling in endothelial disorders. *Current atherosclerosis reports*. 2016;18:31
26. Wilkerson BA, Grass GD, Wing SB, Argraves WS, Argraves KM. Sphingosine 1-phosphate (s1p) carrier-dependent regulation of endothelial barrier: High density lipoprotein (hdl)-s1p prolongs endothelial barrier enhancement as compared with albumin-s1p via effects on levels, trafficking, and signaling of s1p1. *J Biol Chem*. 2012;287:44645-44653
27. Galvani S, Sanson M, Blaho VA, Swendeman SL, Conger H, Dahlback B, Kono M, Proia RL, Smith JD, Hla T. Hdl-bound sphingosine 1-phosphate acts as a biased agonist for the endothelial cell receptor s1p1 to limit vascular inflammation. *Science signaling*. 2015;8:ra79
28. Sattler K, Graler M, Keul P, Weske S, Reimann CM, Jindrova H, Kleinbongard P, Sabbadini R, Brocker-Preuss M, Erbel R, Heusch G, Levkau B. Defects of high-density lipoproteins in coronary artery disease caused by low sphingosine-1-phosphate content: Correction by sphingosine-1-phosphate-loading. *Journal of the American College of Cardiology*. 2015;66:1470-1485
29. Sattler K, Lehmann I, Graler M, Brocker-Preuss M, Erbel R, Heusch G, Levkau B. Hdl-bound sphingosine 1-phosphate (s1p) predicts the severity of coronary artery atherosclerosis. *Cellular physiology and biochemistry : international journal*

of experimental cellular physiology, biochemistry, and pharmacology. 2014;34:172-184
30. Frej C, Linder A, Happonen KE, Taylor FB, Lupu F, Dahlback B. Sphingosine 1-phosphate and its carrier apolipoprotein m in human sepsis and in escherichia coli sepsis in baboons. *Journal of cellular and molecular medicine*. 2016;20:1170-1181
31. Plomgaard P, Dullaart RP, de Vries R, Groen AK, Dahlback B, Nielsen LB. Apolipoprotein m predicts pre-beta-hdl formation: Studies in type 2 diabetic and nondiabetic subjects. *Journal of internal medicine*. 2009;266:258-267
32. Ruiz M, Frej C, Holmer A, Guo LJ, Tran S, Dahlback B. High-density lipoprotein-associated apolipoprotein m limits endothelial inflammation by delivering sphingosine-1-phosphate to the sphingosine-1-phosphate receptor 1. *Arterioscler Thromb Vasc Biol*. 2017;37:118-129
33. Frej C, Mendez AJ, Ruiz M, Castillo M, Hughes TA, Dahlback B, Goldberg RB. A shift in apom/s1p between hdl-particles in women with type 1 diabetes mellitus is associated with impaired anti-inflammatory effects of the apom/s1p complex. *Arterioscler Thromb Vasc Biol*. 2017;37:1194-1205
34. Yanagida K, Liu CH, Faraco G, Galvani S, Smith HK, Burg N, Anrather J, Sanchez T, Iadecola C, Hla T. Size-selective opening of the blood-brain barrier by targeting endothelial sphingosine 1-phosphate receptor 1. *Proc Natl Acad Sci U S A*. 2017;114:4531–4536
35. Allende ML, Yamashita T, Proia RL. G-protein-coupled receptor s1p1 acts within endothelial cells to regulate vascular maturation. *Blood*. 2003;102:3665-3667
36. Pitulescu ME, Schmidt I, Benedito R, Adams RH. Inducible gene targeting in the neonatal vasculature and analysis of retinal angiogenesis in mice. *Nature protocols*. 2010;5:1518-1534
37. Kamii H, Tominaga T. Filament perforation subarachnoid hemorrhage: Mouse model. *Animal Models of Acute Neurological Injuries (Chen J, Xu X-M, Xu ZC, Zhang JH, editors). Humana Press, Totowa, NJ*. 2009;Chapter 23:279-286
38. Kluk MJ, Ryan KP, Wang B, Zhang G, Rodig SJ, Sanchez T. Sphingosine-1-phosphate receptor 1 in classical hodgkin lymphoma: Assessment of expression and role in cell migration. *Lab Invest*. 2013;93:462-471
39. Lee YK, Smith HK, Yuan H, Ito A, Sanchez T. An optimized method for the isolation and the molecular characterization of cerebral microvessels in vivo. *BioRxiv 335224 [Preprint]*. June 13 2018;Available from: https://doi.org/10.1101/335224
40. Sugawara T, Ayer R, Jadhav V, Zhang JH. A new grading system evaluating bleeding scale in filament perforation subarachnoid hemorrhage rat model. *Journal of neuroscience methods*. 2008;167:327-334
41. Liu Y, Jennings NL, Dart AM, Du XJ. Standardizing a simpler, more sensitive and accurate tail bleeding assay in mice. *World journal of experimental medicine*. 2012;2:30-36
42. Parra A, McGirt MJ, Sheng H, Laskowitz DT, Pearlstein RD, Warner DS. Mouse model of subarachnoid hemorrhage associated cerebral vasospasm: Methodological analysis. *Neurol Res*. 2002;24:510-516
43. Vellimana AK, Milner E, Azad TD, Harries MD, Zhou ML, Gidday JM, Han BH, Zipfel GJ. Endothelial nitric oxide synthase mediates endogenous protection against subarachnoid hemorrhage-induced cerebral vasospasm. *Stroke*. 2011;42:776-782
44. Adachi M, Feigin I. Cerebral oedema and the water content of normal white matter. *Journal of neurology, neurosurgery, and psychiatry*. 1966;29:446-450

45. Lu C, Zhu F, Cho YY, Tang F, Zykova T, Ma WY, Bode AM, Dong Z. Cell apoptosis: Requirement of h2ax in DNA ladder formation, but not for the activation of caspase-3. *Mol Cell*. 2006;23:121-132
46. Sharma A, Singh K, Almasan A. Histone h2ax phosphorylation: A marker for DNA damage. *Methods Mol Biol*. 2012;920:613-626
47. Armulik A, Genove G, Mae M, Nisancioglu MH, Wallgard E, Niaudet C, He L, Norlin J, Lindblom P, Strittmatter K, Johansson BR, Betsholtz C. Pericytes regulate the blood-brain barrier. *Nature*. 2010;468:557-561
48. Shi Y, Zhang L, Pu H, Mao L, Hu X, Jiang X, Xu N, Stetler RA, Zhang F, Liu X, Leak RK, Keep RF, Ji X, Chen J. Rapid endothelial cytoskeletal reorganization enables early blood–brain barrier disruption and long-term ischaemic reperfusion brain injury. *Nature communications*. 2016;7:10523
49. Uyama O, Okamura N, Yanase M, Narita M, Kawabata K, Sugita M. Quantitative evaluation of vascular permeability in the gerbil brain after transient ischemia using evans blue fluorescence. *J Cereb Blood Flow Metab*. 1988;8:282-284
50. Cahalan SM, Gonzalez-Cabrera PJ, Sarkisyan G, Nguyen N, Schaeffer MT, Huang L, Yeager A, Clemons B, Scott F, Rosen H. Actions of a picomolar short-acting s1p(1) agonist in s1p(1)-egfp knock-in mice. *Nat Chem Biol*. 2011;7:254-256
51. Rios M, Fan G, Fekete C, Kelly J, Bates B, Kuehn R, Lechan RM, Jaenisch R. Conditional deletion of brain-derived neurotrophic factor in the postnatal brain leads to obesity and hyperactivity. *Mol Endocrinol*. 2001;15:1748-1757
52. Kim GS, Yang L, Zhang G, Zhao H, Selim M, McCullough LD, Kluk MJ, Sanchez T. Critical role of sphingosine-1-phosphate receptor-2 in the disruption of cerebrovascular integrity in experimental stroke. *Nature communications*. 2015;6:7893
53. Kim GS, Jung JE, Niizuma K, Chan PH. Ck2 is a novel negative regulator of nadph oxidase and a neuroprotectant in mice after cerebral ischemia. *J Neurosci*. 2009;29:14779-14789
54. Zhang G, Yang L, Kim GS, Ryan K, Lu S, O'Donnell RK, Spokes K, Shapiro N, Aird WC, Kluk MJ, Yano K, Sanchez T. Critical role of sphingosine-1-phosphate receptor 2 (s1pr2) in acute vascular inflammation. *Blood*. 2013;122:443-455
55. Shih SC, Smith LE. Quantitative multi-gene transcriptional profiling using real-time pcr with a master template. *Exp Mol Pathol*. 2005;79:14-22
56. Montesano R, Pepper MS, Mohle-Steinlein U, Risau W, Wagner EF, Orci L. Increased proteolytic activity is responsible for the aberrant morphogenetic behavior of endothelial cells expressing the middle t oncogene. *Cell*. 1990;62:435-445
57. Muroi C, Fujioka M, Marbacher S, Fandino J, Keller E, Iwasaki K, Mishima K. Mouse model of subarachnoid hemorrhage: Technical note on the filament perforation model. *Acta Neurochir Suppl*. 2015;120:315-320
58. Knowland D, Arac A, Sekiguchi KJ, Hsu M, Lutz SE, Perrino J, Steinberg GK, Barres BA, Nimmerjahn A, Agalliu D. Stepwise recruitment of transcellular and paracellular pathways underlies blood-brain barrier breakdown in stroke. *Neuron*. 2014;82:603-617
59. Swendeman SL, Xiong Y, Cantalupo A, Yuan H, Burg N, Hisano Y, Cartier A, Liu CH, Engelbrecht E, Blaho V, Zhang Y, Yanagida K, Galvani S, Obinata H, Salmon JE, Sanchez T, Di Lorenzo A, Hla T. An engineered s1p chaperone attenuates hypertension and ischemic injury. *Science signaling*. 2017;10

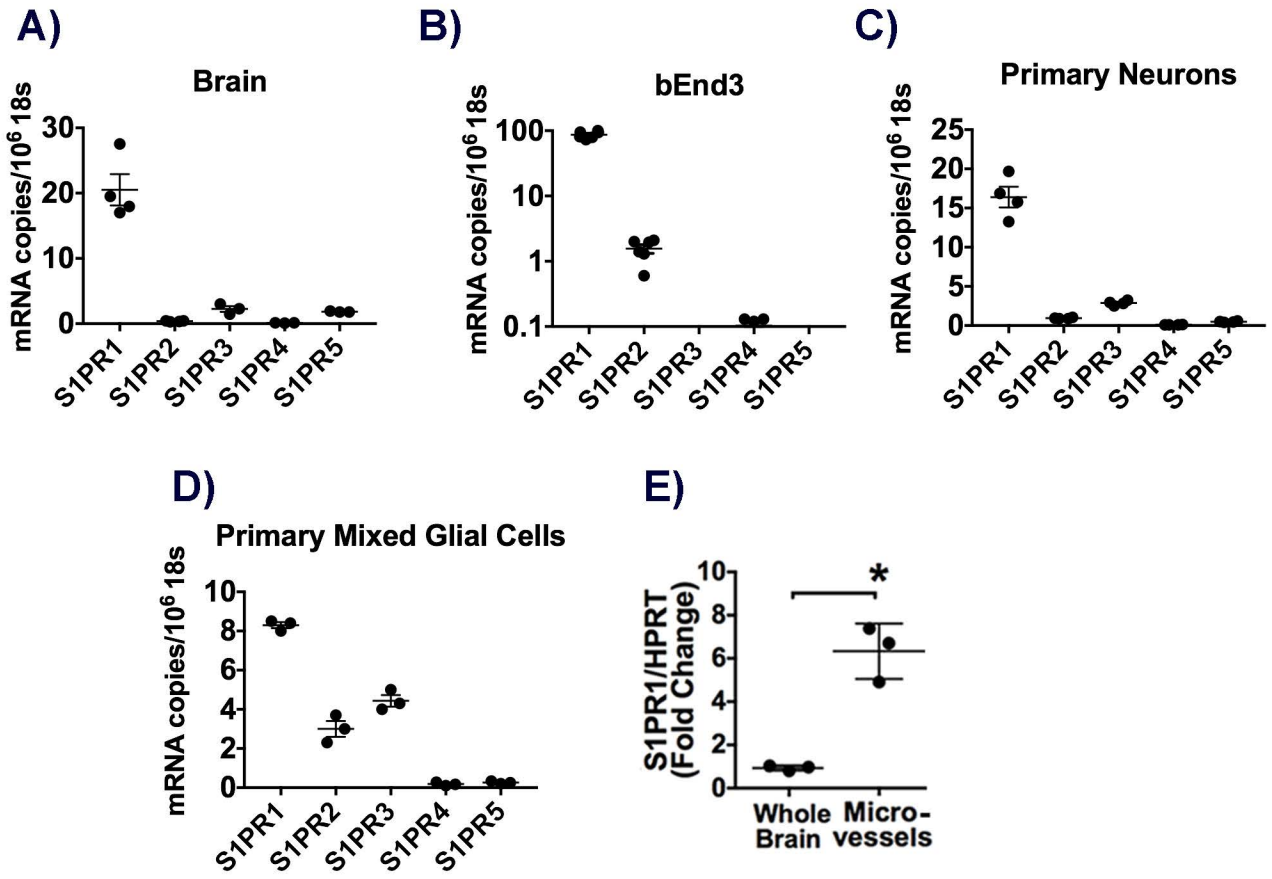
A)
Brain
mRNA copies/10^6 18s
30
20
10
0
S1PR1
S1PR2
S1PR3
S1PR4
S1PR5
B)
bEnd3
mRNA copies/10^6 18s
100
10
1
0.1
S1PR1
S1PR2
S1PR3
S1PR4
S1PR5
C)
Primary Neurons
mRNA copies/10^6 18s
25
20
15
10
5
0
S1PR1
S1PR2
S1PR3
S1PR4
S1PR5
D)
Primary Mixed Glial Cells
mRNA copies/10^6 18s
10
8
6
4
2
0
S1PR1
S1PR2
S1PR3
S1PR4
S1PR5
E)
S1PR1/HPRT
(Fold Change)
10
8
6
4
2
0
*
Whole
Brain
Micro-
vessels

Figure 1

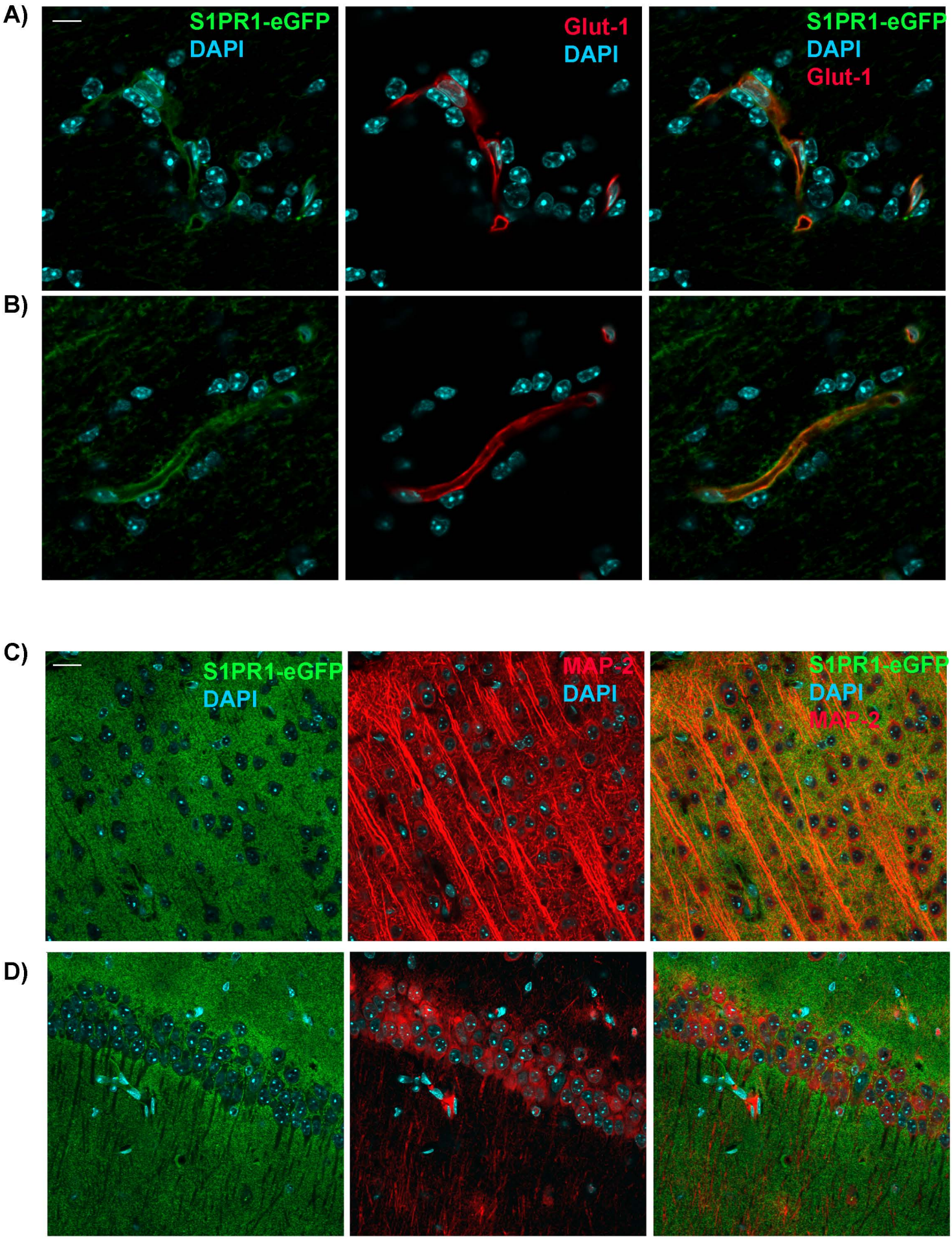
A)
S1PR1-eGFP
DAPI
Glut-1
DAPI
S1PR1-eGFP
DAPI
Glut-1
B)
C)
S1PR1-eGFP
DAPI
MAP-2
DAPI
S1PR1-eGFP
DAPI
MAP-2
D)

Figure 2

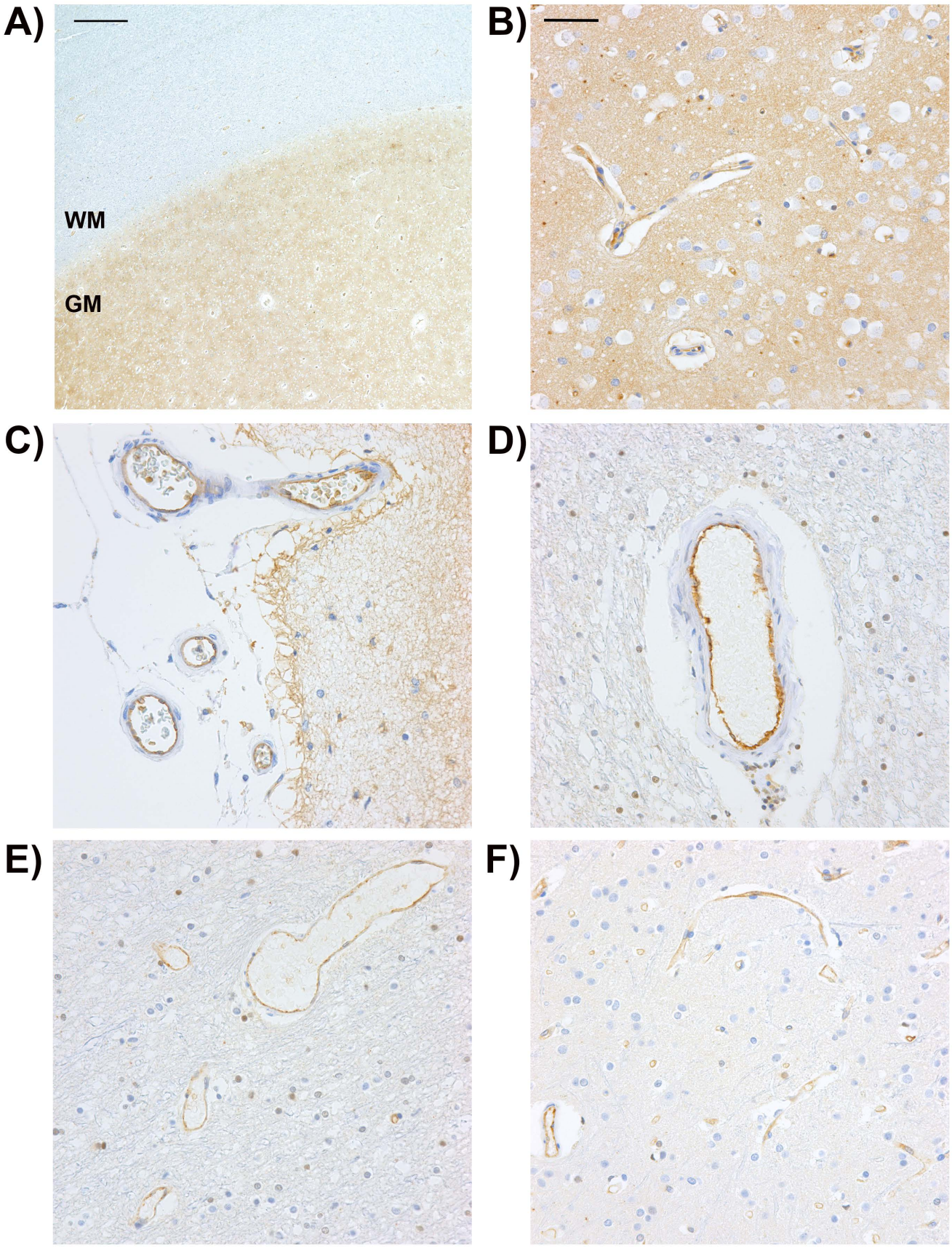

Figure 3

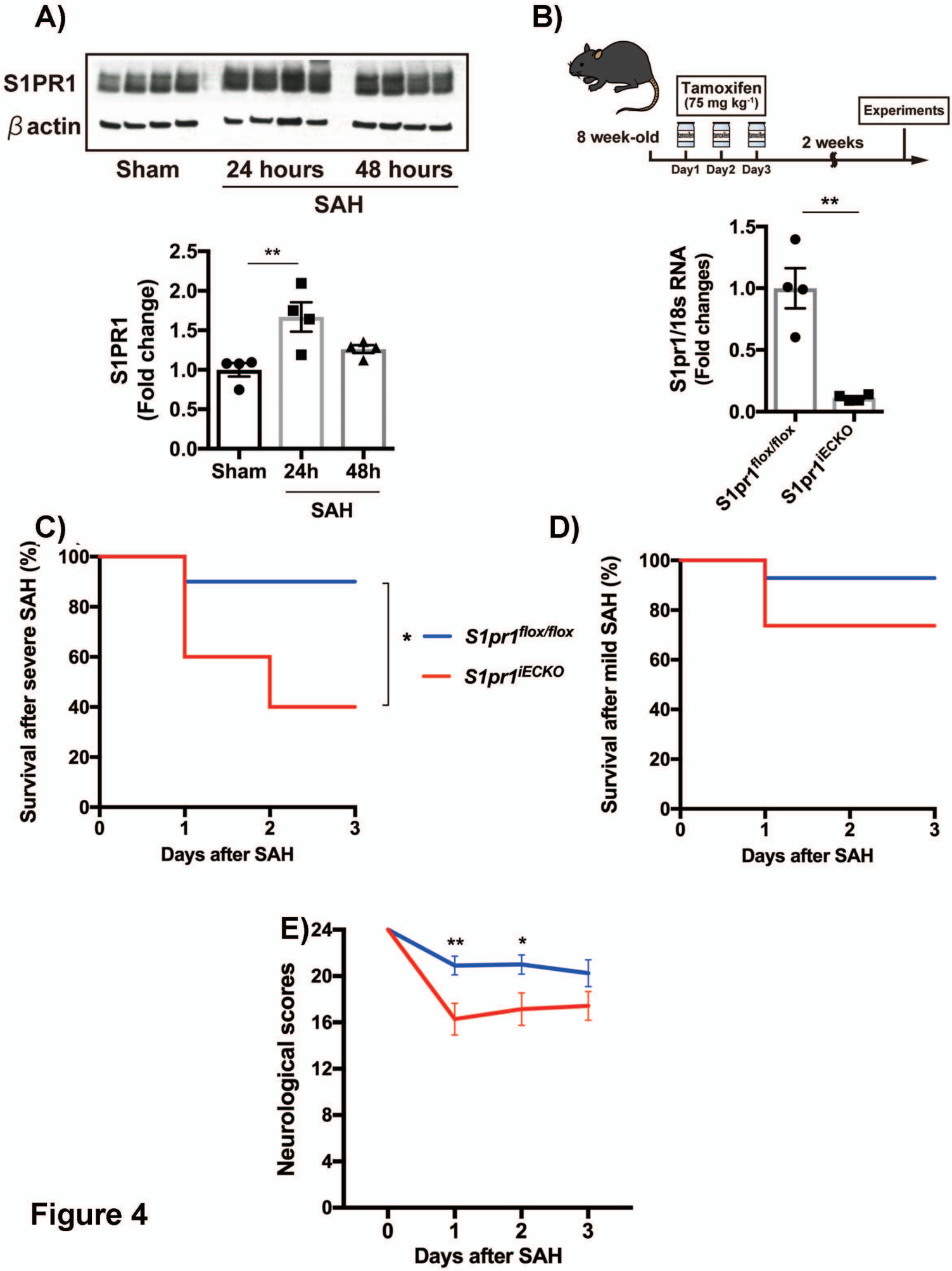
A)
S1PR1
β actin
Sham
24 hours
48 hours
SAH
S1PR1 (Fold change)
2.5
2.0
1.5
1.0
0.5
0.0
**
Sham
24h
48h
SAH
B)
Tamoxifen (75 mg kg-1)
Experiments
8 week-old
2 weeks
Day1 Day2 Day3
**
S1pr1/18s RNA (Fold changes)
1.5
1.0
0.5
0.0
S1pr1flox/flox
S1pr1iECKO
C)
Survival after severe SAH (%)
100
80
60
40
20
0
0
1
2
3
Days after SAH
*
S1pr1flox/flox
S1pr1iECKO
D)
Survival after mild SAH (%)
100
80
60
40
20
0
0
1
2
3
Days after SAH
E)
Neurological scores
24
20
16
12
8
4
0
**
*
0
1
2
3
Days after SAH

Figure 4

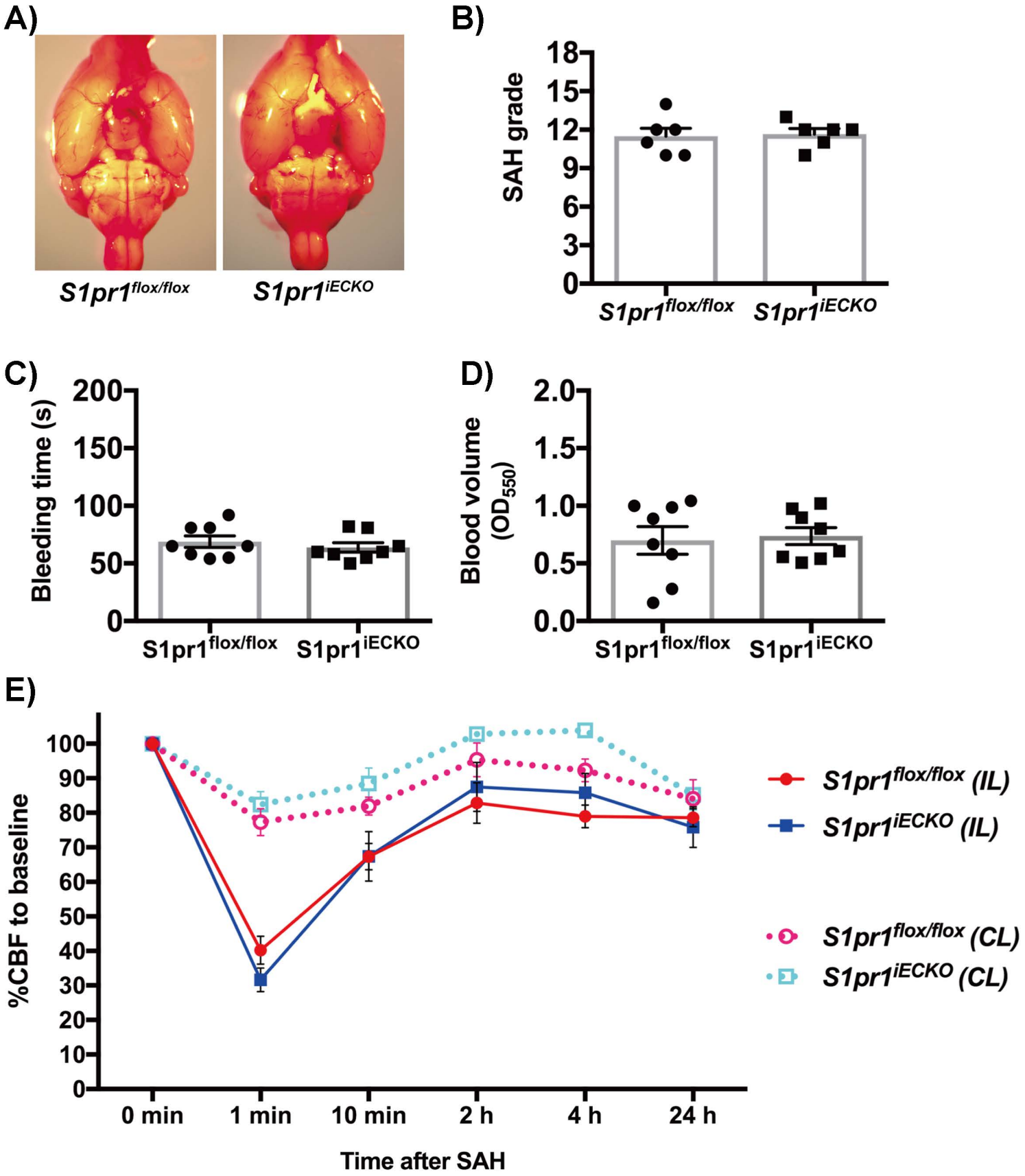
A)
S1pr1flox/flox
S1pr1iECKO
B)
SAH grade
18
15
12
9
6
3
0
S1pr1flox/flox
S1pr1iECKO
C)
Bleeding time (s)
200
150
100
50
0
S1pr1flox/flox
S1pr1iECKO
D)
Blood volume (OD550)
2.0
1.5
1.0
0.5
0.0
S1pr1flox/flox
S1pr1iECKO
E)
%CBF to baseline
100
90
80
70
60
50
40
30
20
10
0
0 min
1 min
10 min
2 h
4 h
24 h
Time after SAH
S1pr1flox/flox (IL)
S1pr1iECKO (IL)
S1pr1flox/flox (CL)
S1pr1iECKO (CL)

Figure 5

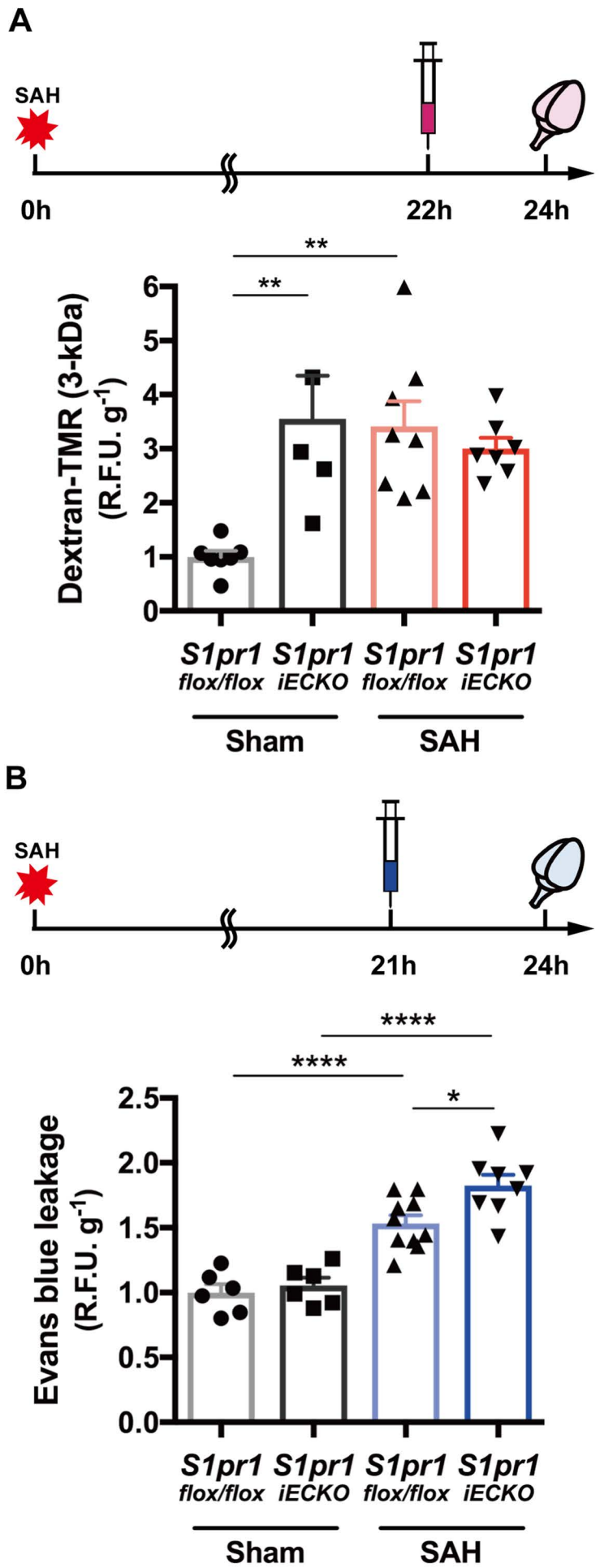
A
SAH
0h
22h
24h
**
**
Dextran-TMR (3-kDa)
(R.F.U. g-1)
0
1
2
3
4
5
6
S1pr1 flox/flox
S1pr1 iECKO
S1pr1 flox/flox
S1pr1 iECKO
Sham
SAH
B
SAH
0h
21h
24h
****
****
*
Evans blue leakage
(R.F.U. g-1)
0.0
0.5
1.0
1.5
2.0
2.5
S1pr1 flox/flox
S1pr1 iECKO
S1pr1 flox/flox
S1pr1 iECKO
Sham
SAH

Figure 6

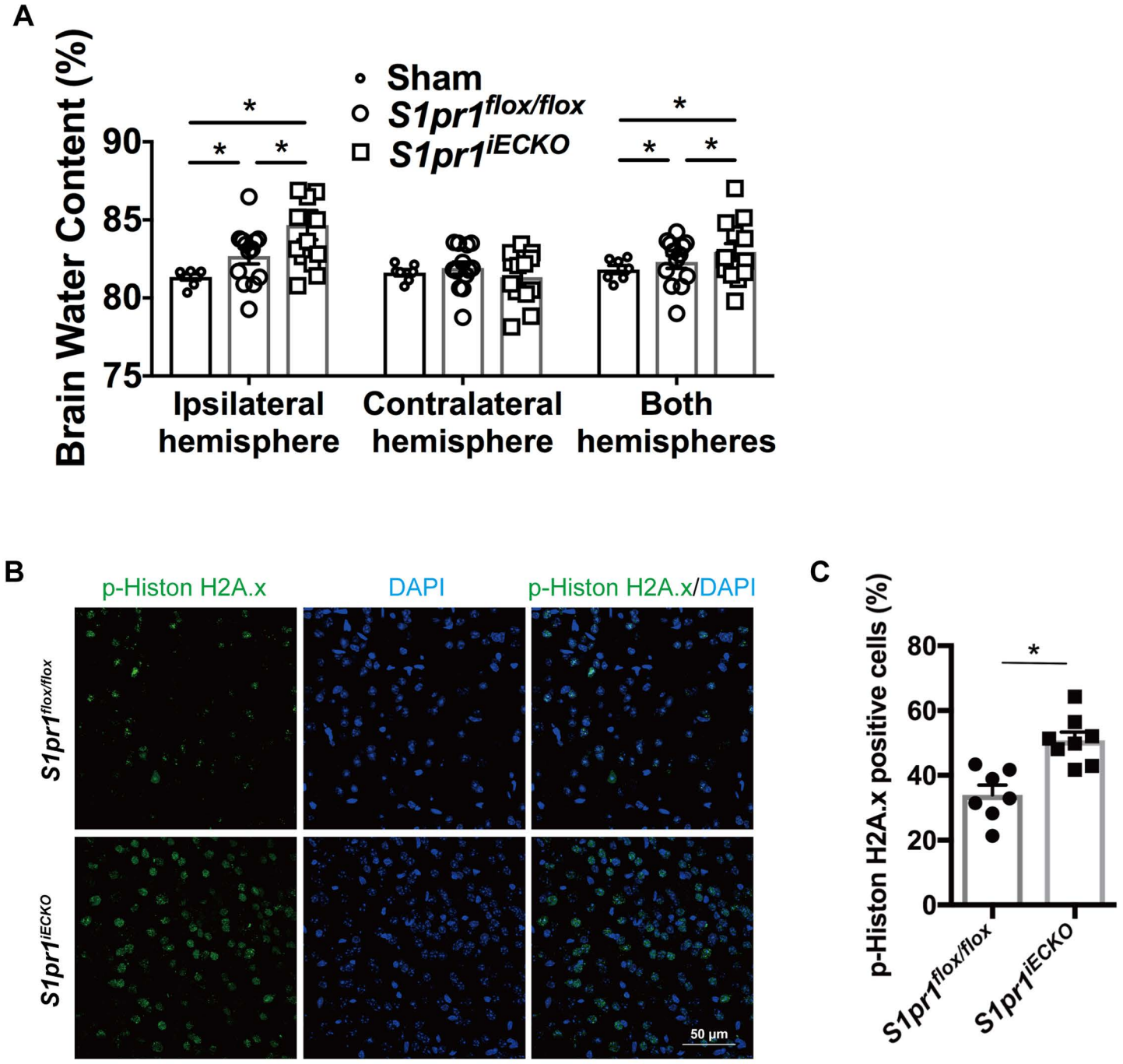
A
Brain Water Content (%)
90
85
80
75
Sham
S1pr1flox/flox
S1pr1iECKO
*
Ipsilateral hemisphere
Contralateral hemisphere
Both hemispheres
B
p-Histon H2A.x
DAPI
p-Histon H2A.x/DAPI
S1pr1flox/flox
S1pr1iECKO
50 μm
C
p-Histon H2A.x positive cells (%)
80
60
40
20
0
S1pr1flox/flox
S1pr1iECKO

Figure 7

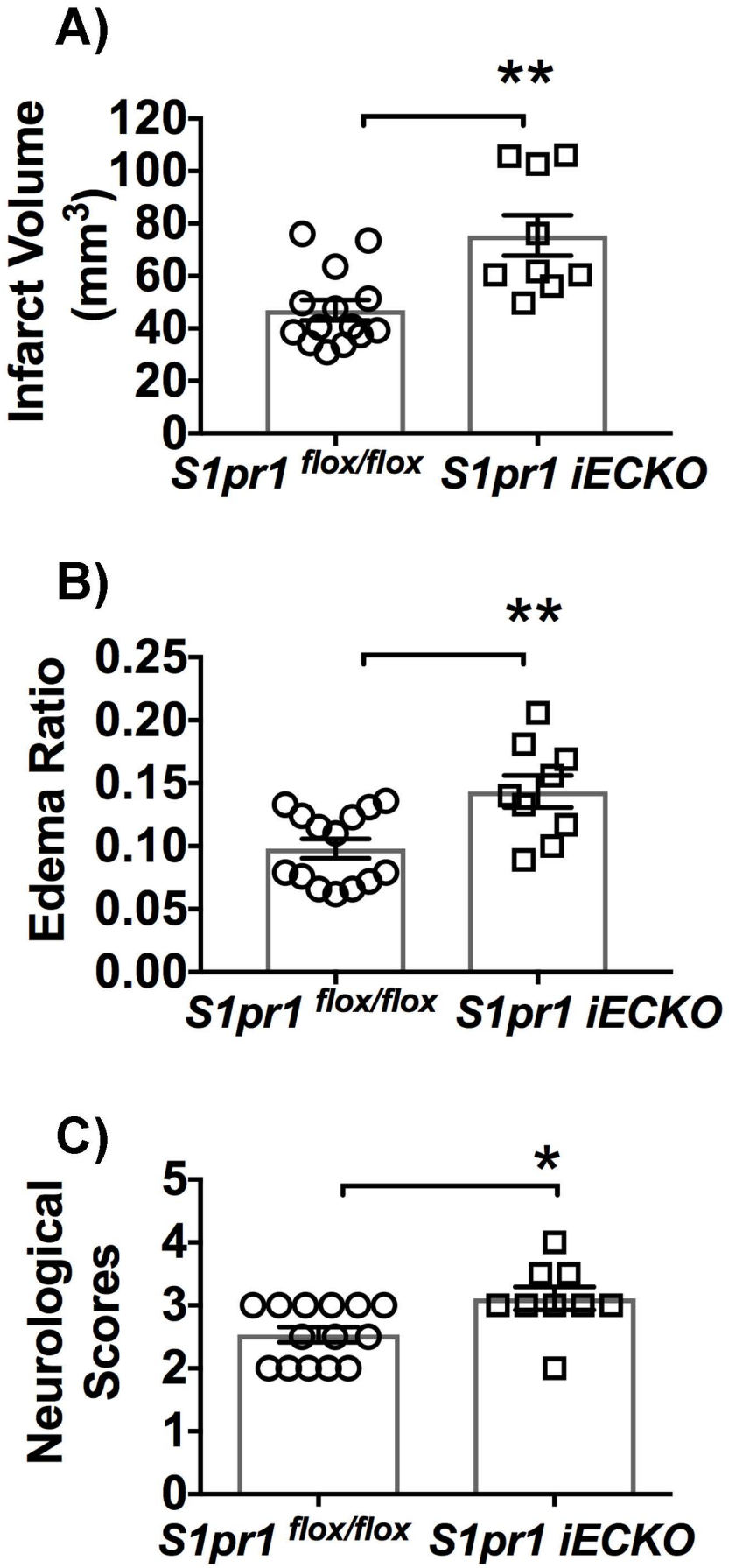
A)
**
Infarct Volume (mm3)
120
100
80
60
40
20
0
S1pr1 flox/flox
S1pr1 iECKO
B)
**
Edema Ratio
0.25
0.20
0.15
0.10
0.05
0.00
S1pr1 flox/flox
S1pr1 iECKO
C)
*
Neurological Scores
5
4
3
2
1
0
S1pr1 flox/flox
S1pr1 iECKO

Figure 8